Slip-weakening distance in dynamic rupture of inslab normal-faulting earthquakes

AUTHOR(S):

Mikumo, Takeshi; Yagi, Yuji

CITATION:

Mikumo, Takeshi ...[et al]. Slip-weakening distance in dynamic rupture of inslab normal-faulting earthquakes. Geophysical Journal International 2003, 155(2): 443-355

ISSUE DATE:

2003-11

URL:

http://hdl.handle.net/2433/193412

Geophys. J. Int. (2003) **155,** 443–455

Slip-weakening distance in dynamic rupture of in-slab normal-faulting earthquakes

Takeshi Mikumo[1] and Yuji Yagi[2]

[1] *Instituto de Geofisica, Universidad Nacional Autonoma de Mexico, Ciudad Universitaria, Mexico* 04510 *D.F., Mexico*
[2] *International Institute for Seismology and Earthquake Engineering, Building Research Institute, Tsukuba, Ibaraki* 305-0802, *Japan*

Accepted 2003 May 21. Received 2003 April 10; in original form 2002 October 9

SUMMARY

We estimate the critical slip-weakening distance on in-slab earthquake faults in a subduction zone, by applying a recent approach proposed by us. This approach is to find a relation between the breakdown time of shear stress T_b, the time of peak slip velocity T_{pv}, and the slip-weakening distance D_c, from the time histories of shear stress, slip and slip velocity at each point on the fault. The previous results show that D_c at T_b can be well approximated by D_c' at T_{pv} for faults even with a heterogeneous stress drop distribution, except at locations near barriers and fault edges.

We apply the above method to three large in-slab, normal-faulting earthquakes in the Mexican subduction zone. To do this, we calculate the spatial distribution of slip-velocity functions and final slip from kinematic waveform inversion of strong-motion and teleseismic records, and the stress history and final stress change from dynamic rupture calculations. By integrating the slip-velocity functions obtained from the inversion, from the rupture arrival time to the time of peak slip velocity, we obtain slip D_c' at T_{pv} and then correct it for D_c at T_b through dynamic calculations. We also estimate the lowest resolvable limit and probable errors of D_c from the slip-velocity functions, and its upper bound from a theoretical constraint between the dynamic stress drop and D_c. We found that the slip-weakening distance D_c estimated in the frequency band between 0.05 and 0.5 Hz ranges between 40 and 120 cm on the in-slab fault of the 1999 Oaxaca earthquake ($M_w = 7.5$). The largest D_c is detected in the central fault and in part of the deeper sections, and D_c in the zone around the hypocentre ranges between 50 and 70 cm. The estimated D_c values appear to be less depth-dependent but are rather more dependent on the local maximum slip. This possible slip dependence might be interpreted by the degree of fault roughness, in addition to stress heterogeneities. The fracture energy G in the central section and in the hypocentral zone are roughly estimated to be of the order of 10–15 and 5–8 MJ m^{-2}, respectively. Both of the estimated D_c and G values are somewhat larger than those on the vertical fault of two recent, shallow strike-slip earthquakes in western Japan.

Key words: dynamic rupture, in-slab faults, normal-faulting earthquakes, slip-weakening.

1 INTRODUCTION

It has been demonstrated by both theoretical studies (e.g. Ida 1972; Andrews 1976a,b; Day 1982; Ohnaka & Yamashita 1989; Matsu'ura *et al.* 1992; Fukuyama & Madariaga 1998; Madariaga *et al.* 1998; Shibazaki & Matsu'ura 1998; Campillo *et al.* 2001) and laboratory experiments (e.g. Dieterich 1981; Okubo & Dieterich 1984; Ohnaka *et al.* 1987; Ohnaka & Kuwahara 1990; Ohnaka & Shen 1999) that the constitutive frictional relations, particularly the slip-weakening behaviour of shear stress, play a critical role in the dynamic part of the rupture process and hence on strong ground motions during large earthquakes. Accordingly, it is now one of the important issues in rupture dynamics to estimate the critical slip-weakening distance at which the shear stress drops to the final frictional level during natural earthquakes.

For actual earthquakes, several attempts have been made to date to infer the slip-weakening distance D_c by various methods (Papageorgiou & Aki 1983; Ide & Takeo 1997; Olsen *et al.* 1997; Day *et al.* 1998; Guatteri & Spudich 2000; Ohnaka 2000; Pulido & Irikura 2000; Peyrat *et al.* 2001). It seems, however, that some of the D_c values may be overestimated due to limited data resolution, although D_c may be a significant fraction of the maximum slip on the fault.

More recently, Mikumo *et al.* (2003) estimated the critical slip-weakening distance on earthquake faults, by applying a new approach that is independent of the estimate of fracture energy or

radiated seismic energy. In this approach, dynamic calculations provided a physically based relation between the breakdown time of shear stress T_b, the time of peak slip velocity T_{pv} and the prescribed slip-weakening distance D_c at each point on the fault. The validity of the method has been justified by Fukuyama *et al.* (2003) based on the theoretical background for the shear traction on a 2-D fault given by boundary integral equations in Fukuyama & Madariaga (1998). It has been shown that T_b is well approximated by T_{pv} except at points near fault edges and strong barriers, and that D_c at time T_b may be estimated from slip D'_c at time T_{pv} after some corrections. The above method has been applied to two strike-slip earthquakes in western Japan, the 2000 Tottori and the 1995 Kobe earthquakes, by estimating T_{pv} in the slip-velocity functions on the vertical fault obtained from kinematic waveform inversion of strong-motion and teleseismic records. From these procedures, Mikumo *et al.* (2003) found that the slip-weakening distance D_c estimated in the frequency window between 0.05 and 0.5 Hz ranges between 40 and 90 cm in the major part of the two earthquake faults. Referring to this method, Olsen *et al.* (2003) also estimated the average D_c on the Tottori earthquake fault from direct measurement of near-fault strong-motion waveforms. However, all of the above estimates may have quite large uncertainties, considering the limited frequency resolution of the observed waveforms, probable time errors in the slip-velocity function and the uncertainty of the slip-weakening behaviour. Nevertheless, it is still interesting to note that the estimated D_c values appear to be spatially variable and dependent on the local maximum slip.

The findings from this approach as well as several previous attempts were all for strike-slip earthquakes in the shallow part of the continental crust. There still remains a question as to what extent the slip-weakening distance scales with the size of the fault zone and varies with its environments, particularly for large interplate thrust and in-slab normal-faulting earthquakes in subduction zones. In the present paper, we focus our attention on three in-slab normal-faulting earthquakes in the Mexican subduction zone by applying an approach similar to that of Mikumo *et al.* (2003), with an additional theoretical constraint between dynamic stress drop and the slip-weakening distance on the fault. To do this, we calculate the spatial distribution of slip-velocity functions and final slip on the in-slab fault from kinematic waveform inversion of strong-motion and teleseismic data, and the stress history and final stress change from dynamic calculations.

2 IN-SLAB NORMAL-FAULTING EARTHQUAKES IN THE MEXICAN SUBDUCTION ZONE

In the Mexican subduction zone, large interplate thrust earthquakes frequently occur on the upper interface of the subducting Cocos plate (e.g. Singh *et al.* 1981; Pardo & Suarez 1995), while large normal-faulting earthquakes also take place within the subducting slab. These in-slab events occur mainly far down-dip in its unbending or subhorizontal portion at some distances away from the trench (e.g. Singh *et al.* 1999), but in some cases below the ruptured fault zone of preceding large thrust earthquakes (Singh *et al.* 1985; Cocco *et al.* 1997; Mikumo *et al.* 1999, 2002). In the present study, we deal mainly with the rupture dynamics of the 1999 Oaxaca earthquake ($M_w = 7.5$) that occurred below the down-dip edge of the 1978 thrust earthquake fault ($M_w = 7.8$). In addition, we also investigate the 1999 Tehuacan earthquake ($M_w = 7.0$), which took place in the unbending portion of the subducted plate, and the 1997 normal-faulting event ($M_w = 7.1$) that occurred beneath the ruptured area of the 1985 Michoacan thrust earthquake ($M_w = 8.1$). For these earthquakes, the source mechanism and slip distribution on the fault have been analysed using well-recorded local, regional and teleseismic data. Possible stress interactions have also been suggested between the preceding thrust and the following two normal-faulting earthquakes (Mikumo *et al.* 1999, 2002).

1999 Oaxaca earthquake

The mainshock hypocentre of the 1999 September 30 Oaxaca earthquake was located at 16.00°N and 97.02°W at a depth of 40 km from the local broad-band seismic network (Singh *et al.* 2000) (see Fig. 1a). The centroid moment tensor solutions given by different institutions provided two nodal planes; I ($\delta = 51°$–$55°$, $\phi = 295°$–$315°$, slip $= -81°$ to $-83°$) and II ($\delta = 36°$–$40°$, $\phi = 103°$–$120°$, slip $= -99°$ to $-102°$), indicating a normal-faulting mechanism, with the epicentral location and focal depth somewhat deviated from the local observations. The estimated seismic moment ranges between 1.3 and 2.0 $\times 10^{27}$ dyn cm. The kinematic inversion has been performed from 21 strong-motion records from seven local stations (Hernandez *et al.* 2001), together with 15 teleseismic *P* waveforms (Yagi *et al.* 2001). The two analyses, both referring to the focal

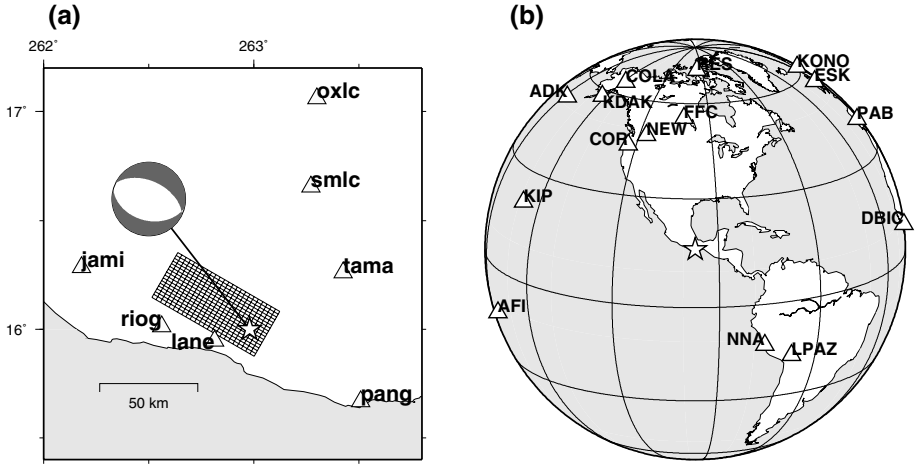

Figure 1. (a) Location of the 1999 Oaxaca, Mexico, earthquake ($M_w = 7.4$) with its fault-plane solution, broad-band and strong-motion stations in the surrounding region, which are used in the kinematic waveform inversion. (b) Location of teleseismic stations used for the kinematic waveform inversion.

depth of 40 km, give a smaller misfit between the recorded and synthetic waveforms for a northeastward-dipping nodal plane than for the other. This indicates that the 1999 Oaxaca earthquake was a normal-faulting event with the fault plane dipping at about 50° toward inland in the subducting Cocos plate. The slip distribution on the fault plane given by Hernandez *et al.* (2001) shows two areas with a maximum slip around 2.5 m at depths between 40 and 55 km and an area with a smaller slip of 2 m around the hypocentre. On the other hand, Yagi *et al.* (2001) provided the fault extending from 34 to 62 km with a maximum slip of 2.3 m at depths between 47 and 52 km, and with a smaller slip of 1.4 m near the hypocentre.

Slip distribution from kinematic waveform inversion

To discuss the slip-weakening distance from the stress-breakdown time during the dynamic fault rupture, we performed more detailed, kinematic waveform inversion than the previous inversion by Yagi *et al.* (2001). The data used for our present purpose are 21 strong-motion records from seven local and regional stations (Fig. 1a) and 15 long-period *P* waveforms from 15 teleseismic stations (Fig. 1b). The strong-motion records were bandpass-filtered between 0.05 and 0.5 Hz and numerically integrated to ground displacement with a sampling interval of 0.25 s, while the teleseismic data were bandpass-filtered between 0.005 and 1 Hz and integrated to ground displacement with a sampling interval of 0.25 s. For this procedure, we applied a fourth-order Butterworth filter to remove low-frequency noise arising from the integration and high-frequency waves above 0.5–1.0 Hz for which the Green's function for local minor velocity structures is not well known. For the inversion analysis, the entire fault plane with dimensions of 60 × 40 km^2 was divided into 384 subfaults each having a size of 2.5 × 2.5 km^2. The crust and uppermost mantle structures used here are given in Table 1 for the Oaxaca region and in Table 2 for teleseismic receiver stations. The Green's functions for all subfault to local and regional station pairs were calculated by the discrete wavenumber method developed by Koketsu (1985), while the functions for teleseismic stations were calculated by the method of Kikuchi & Kanampori (1991). The basis source time function on each subfault was expanded into 39 sequential, overlapping triangles, each having a half duration of 0.25 s with a time-shift of 0.25 s, and re-sampled at an interval of 0.05 s. In the inversion procedure, we put relative weights on the recording stations, considering the quality of the records observed at these stations. The weights are taken to be inversely proportional to the standard deviation of the recorded maximum amplitude, which is 50 per cent for the Jami station and 10 per cent for other stations.

The strong-motion and teleseismic displacement waveforms and the corresponding synthetic seismograms obtained from the final inversion are shown in Fig. 2. The observed and synthetic waveforms generally show a very good fit, except for station Jami. The misfit at this station may be due to some site effects. Fig. 3 shows the spatial slip distribution over the fault, which has been revealed from the inversion. It can be seen that there are four large-slip zones; one is located in the central section at depths between 38 and 52 km with a maximum slip of 2.3 m, the second is its downward and rightward continuation at depths between 53 and 60 km, the third one is located around the hypocentre at depths between 38 and 42 km, and the last one is located near the upper right-hand section of the fault.

Recently, Fukahata *et al.* (2003) performed another inversion analysis, by applying Akaike's Bayesian information criterion (ABIC) (Akaike 1980) to the same data set as above. Their results using the more rigorous criterion provided a slip distribution that includes a clear global minimum of the ABIC value. The distribution shows a pattern almost similar to that from the above analysis, suggesting high reliability of the present results. The difference may come from taking into account the quality of the observed records and from the smaller size of subfaults and the shorter duration of the basis function adopted in the present study.

Table 1. Crust and uppermost mantle structure model for the Oaxaca region used in this study.

Layer (no)	H (km)	V_p (km s^{-1})	V_s (km s^{-1})	ρ (g cm^{-3})
1	0	5.30	3.06	2.70
2	5	6.20	3.58	2.75
3	15	6.85	3.95	2.90
4	30	8.15	4.71	3.20

H, top depth to each layer; V_p, P-wave velocity; V_s, S-wave velocity; ρ, density.

Table 2. Crust and upper-mantle structure used for teleseismic receiver stations (Yagi *et al.* 2001).

Layer No.	H (km)	V_p (km s^{-1})	V_s (km s^{-1})	ρ (gr cm^{-3})
1	0	5.57	3.36	2.65
2	15	6.50	3.74	2.87
3	33	8.10	4.68	3.30

For Green's functions, the attenuation terms are included with $T/Q_p = 1.0$ (s) and $T/Q_s = 4.0$ (s).

Spatial distribution of stress change

Next, we calculate the spatial distribution of static stress change from the slip distribution shown in Fig. 3. The procedure follows the approach by Mikumo & Miyatake (1993) for a 3-D dynamic model incorporating a dipping fault embedded in a horizontally layered velocity structure. In this 3-D model, the shear stress is applied along the dipping fault just above and just below it. We solve elastodynamic equations, incorporating the kinematic slip under appropriate boundary conditions with a second-order finite-difference scheme. The boundary conditions imposed here are: (1) the continuity of the normal stress and normal displacement component across the dipping fault; (2) traction-free vertical stress components at the ground surface; (3) the continuity of all stress and displacement components at each of the layer interfaces (Mikumo *et al.* 1987); and (4) the absorbing boundary conditions (Clayton & Engquist 1977) at the side and bottom of the model space. First, we estimate approximate static stress changes from the fault slip using Okada's formulations for a uniform half-space (Okada 1992). Given these stress changes as starting values, we calculate the slip distribution from dynamic rupture propagating with fixed rupture velocities in the layered velocity structure, and then take the ratio between the already obtained kinematic slip and the calculated dynamic slip at each point on the fault. The ratio is multiplied to the previously given static stress drop, and this procedure is repeated until the rms difference between the kinematic and dynamic slips over the fault can be minimized within a reasonably small value.

For numerical calculations, we interpolate the kinematic slip obtained at every 2.5 km into a grid of 1.25 or 0.625 km on the dipping fault. The extent of the 3-D model space is taken as 125 × 85 × 85 km^3, and the grid spacings are 1.250, 0.884 and 0.884 km or 0.625, 0.442 and 0.442 km in the strike direction, the downward vertical direction and in the direction perpendicular to the strike,

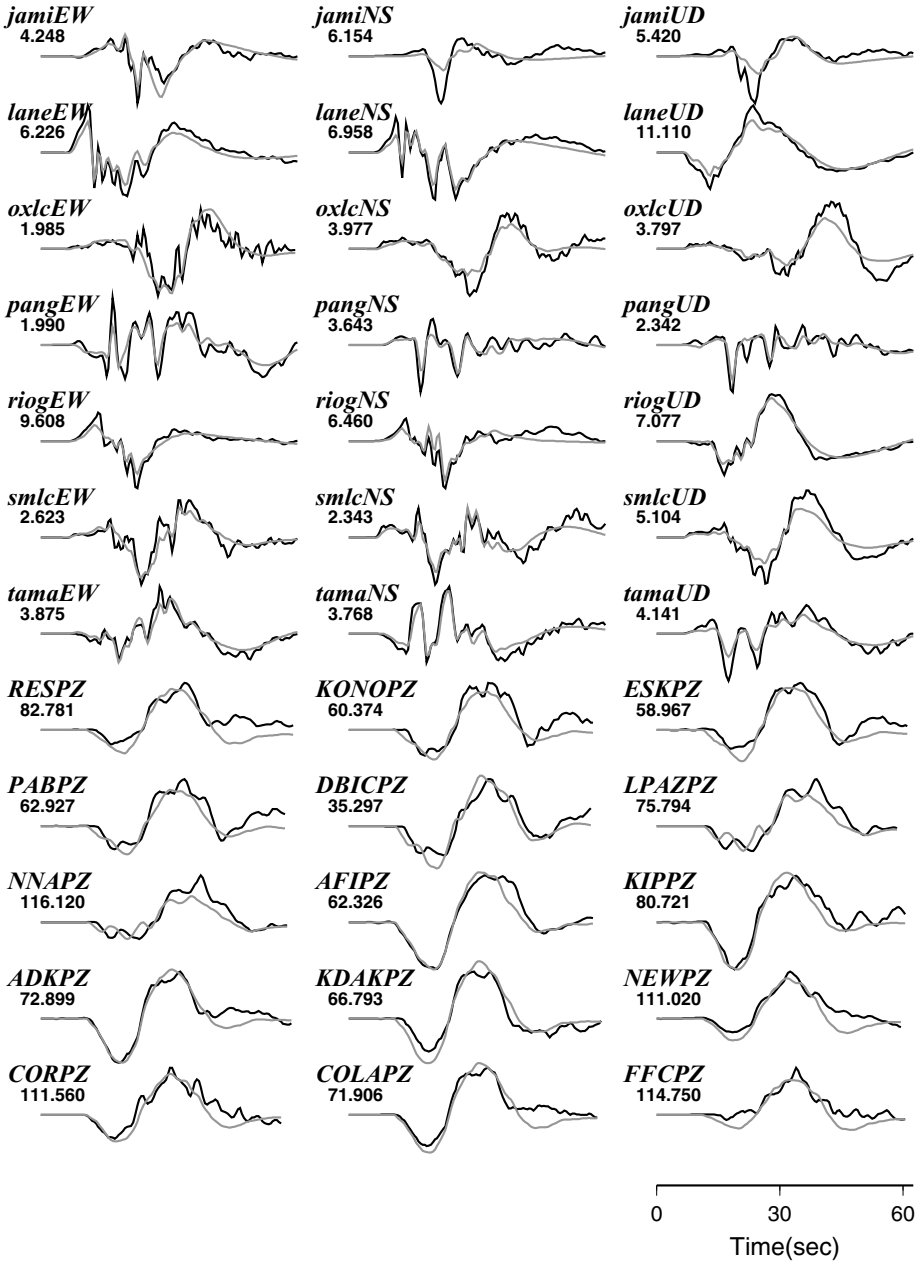

Figure 2. Observed waveforms (thick lines) recorded at near-field broad-band and strong-motion stations and teleseismic stations, and the corresponding synthetic seismograms (thin lines) calculated from the inversion. The numerals below the near-field and teleseismic station codes indicate the maximum amplitude in centimetres and micrometres, respectively.

respectively. Fig. 4 shows the spatial distribution of the calculated static stress changes over the fault. The maximum stress drop in the four large-slip zones ranges between 125 and 110 bar (12.5 and 11.0 MPa). In addition, there are three zones of negative stress drop (a stress increase up to a maximum of 70 bar or 7 MPa) corresponding to smaller-slip zones adjacent to large-slip zones. The spatial distribution of final slip and stress change derived here is used as observational constraints in the next section.

Estimate of D_c from the slip-velocity functions

In order to estimate the slip-weakening distance during dynamic fault rupture, we follow the approach introduced by Mikumo *et al.* (2003) using the slip-velocity functions on the fault. Fig. 5(a) illustrates a simple slip-weakening behaviour proposed by Andrews (1976a,b), where the initial stress σ_0 at each point on a 2-D fault increases up to the yield stress σ_y as the rupture front approaches, and then decreases linearly with ongoing slip down to the final stress σ_f, although there could be different slip-weakening behaviours as suggested by Ida (1972), Ohnaka & Yamashita (1989), Matsu'ura *et al.* (1992) and Campillo *et al.* (2001). One of the previous dynamic calculations on a vertical fault (Mikumo *et al.* 2003), incorporating the above simple slip-weakening law, yield typical time histories of shear stress, slip and slip velocity at a location on the fault, as depicted in Fig. 5(b). The slip velocity starts to evolve as the shear stress increases due to the arrival of the rupture front at

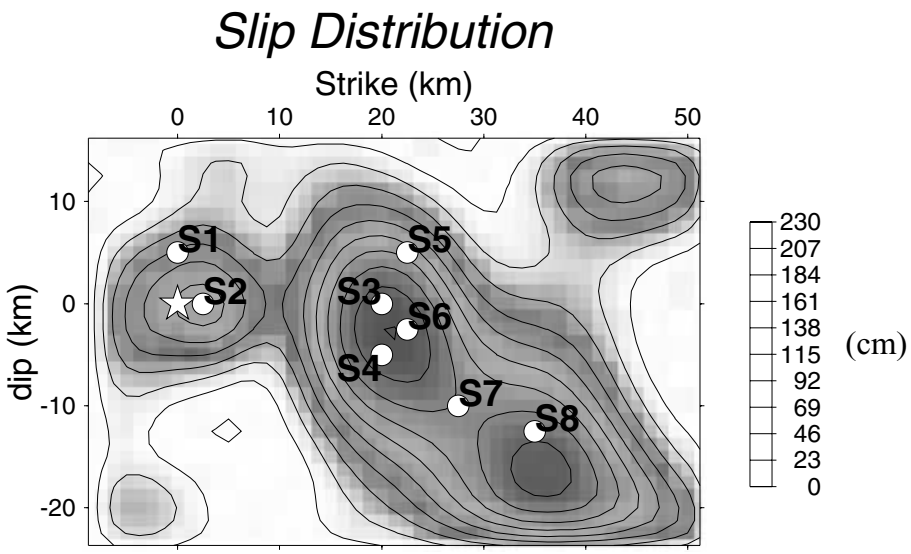

Figure 3. Spatial distribution of slip obtained from the kinematic waveform inversion. S1–S8 are the selected locations where the calculated slip-velocity functions are shown in Fig. 6. The star indicates the hypocentre location.

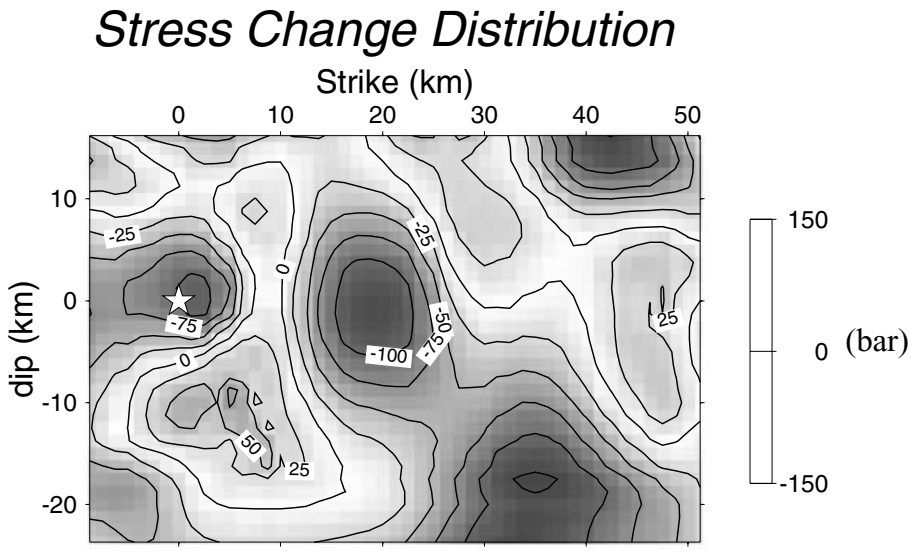

Figure 4. Spatial distribution of stress change calculated from the slip distribution. Dark-shaded zones including contours with minus sign indicate the zone of static stress drop, and light-shaded zones including contours with a plus sign indicate the zones of stress increase.

time T_r, and then reaches the peak value at time T_{pv} as the stress drops from its yield value. However, T_{pv} deviates slightly from the stress-breakdown time T_b, and hence the slip D_c' at T_{pv} is somewhat different from the slip-weakening distance D_c at T_b. This typical behaviour is almost similar for the dipping fault in the present case.

Fig. 6 shows examples of the slip-velocity time functions at eight selected points on the in-slab fault, which have been obtained at every 0.05 s to match the synthetics to the recorded waveforms (Fig. 2) by the kinematic waveform inversion described in the foregoing section. To estimate D_c' from these slip-velocity functions, we numerically integrate the time functions from the time of rupture arrival T_r to the time of the peak slip velocity T_{pv} on each subfault, where T_r has been obtained within an error of 0.25 s in the inversion. The calculations were made only for subfaults having slip greater than 40 cm and slip velocity greater than 30 cm s^{-1} to use reliable slip-velocity functions. The functions contaminated by minor spurious oscillations or having unusual shapes were excluded. The estimated D_c' values are found to be in the range between 40 and 120 cm.

To make corrections on the D_c' values for estimating the actual slip-weakening distance D_c, we perform dynamic calculations imposed with the four boundary conditions described in the previous section, incorporating the final slip shown in Fig. 3 and the stress change shown in Fig. 4 as observational constraints. These calculations are performed with the slip-weakening conditions introduced by Andrews (1976a,b),

$$\sigma(D) = \sigma_y - (\sigma_y - \sigma_f)D/D_c \quad \text{for} \quad D < D_c$$
$$\sigma(D) = \sigma_f \quad \text{for} \quad D > D_c \tag{1}$$

where D is the current slip, which is the difference between the downward oblique slip on the hanging-wall side and the upward

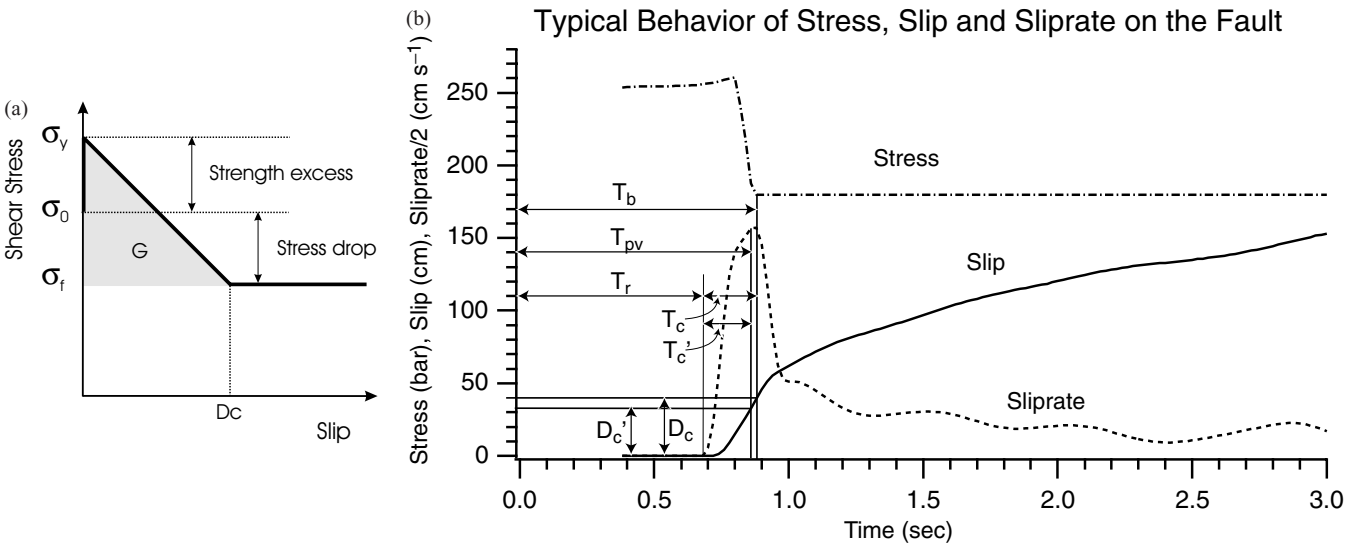

Figure 5. (a) Linear slip-weakening friction law, modified from Andrews (1976a,b). σ_y is the yield stress, σ_0 is the initial stress, σ_f is the final frictional stress. $\sigma_y - \sigma_0$ is defined as the strength excess, $\Delta\sigma_b = \sigma_y - \sigma_f$ is called the breakdown stress drop, and $\Delta\sigma = \sigma_0 - \sigma_f$ is the dynamic stress drop. In this model without dynamic overshooting, the dynamic stress drop is equal to the static stress drop. D_c is defined as the critical slip-weakening distance, and G is the fracture energy, defined as $G = (\sigma_y - \sigma_f)\, D_c/2$. (b) A typical behaviour of the time history of shear stress, slip and slip velocity on the fault. T_b is the breakdown time of stress, T_{pv} is the time of peak slip velocity, D_c is the slip at time T_b, and D_c' is the slip at time T_{pv}.

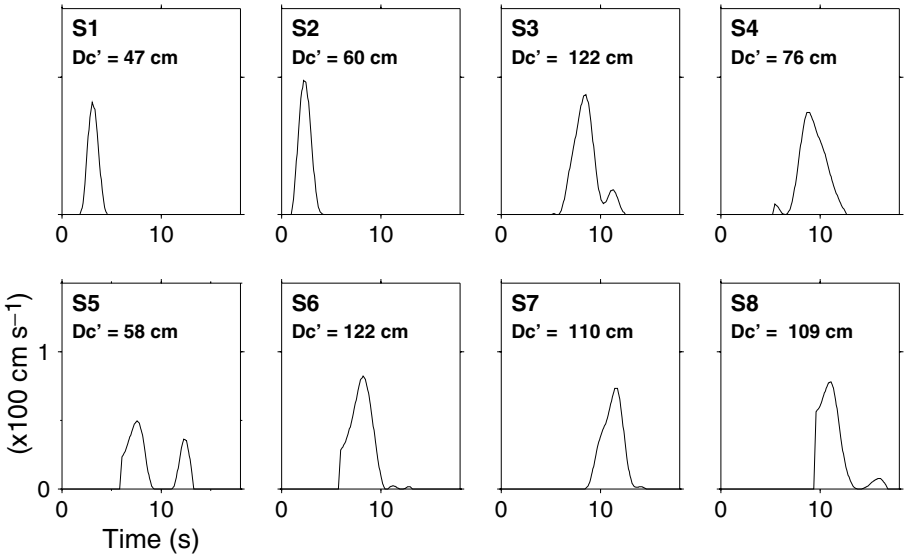

Figure 6. Slip-velocity functions obtained from the kinematic inversion and the estimated D_c' values (cm) at eight selected points (S1–S8) on the in-slab fault shown in Fig. 3.

oblique slip on the footwall side, which occur along the upper interface of the subducting plate. The stress drop $\sigma_0 - \sigma_f$ is taken from Fig. 4, and the strength excess $\sigma_y - \sigma_0$ is roughly estimated during dynamic calculations when the rupture time T_r at each point on the fault is specified (Miyatake 1992) with fixed rupture velocities of $0.7V_s$.

The above dynamic calculations were made for selected points with large slip velocities, for prescribed values of $D_c = 40$ and 80 cm. Fig. 7 shows examples of the calculated time histories of stress change, slip and slip velocity at four selected points. Fig. 8 gives the T_b–T_{pv} relation on the left-hand side and the T_{pv}–D_c' relation on the right-hand side. It can be seen that D_c' estimated from T_{pv} falls between 33 and 47 cm for $D_c = 40$ cm, and between 63 and 77 cm for $D_c = 80$ cm. This indicates that the correction factors D_c/D_c' to obtain D_c from D_c' are within 22 per cent, which are comparable with the probable errors described in the next section. However, it was found that the time histories of both stress change and slip velocity at points close to the lower edge of the fault are strongly affected by the edge effect rather than by the prescribed slip-weakening distance, as has been pointed out by Fukuyama *et al.* (2003). For this reason, these points were excluded from the present analysis.

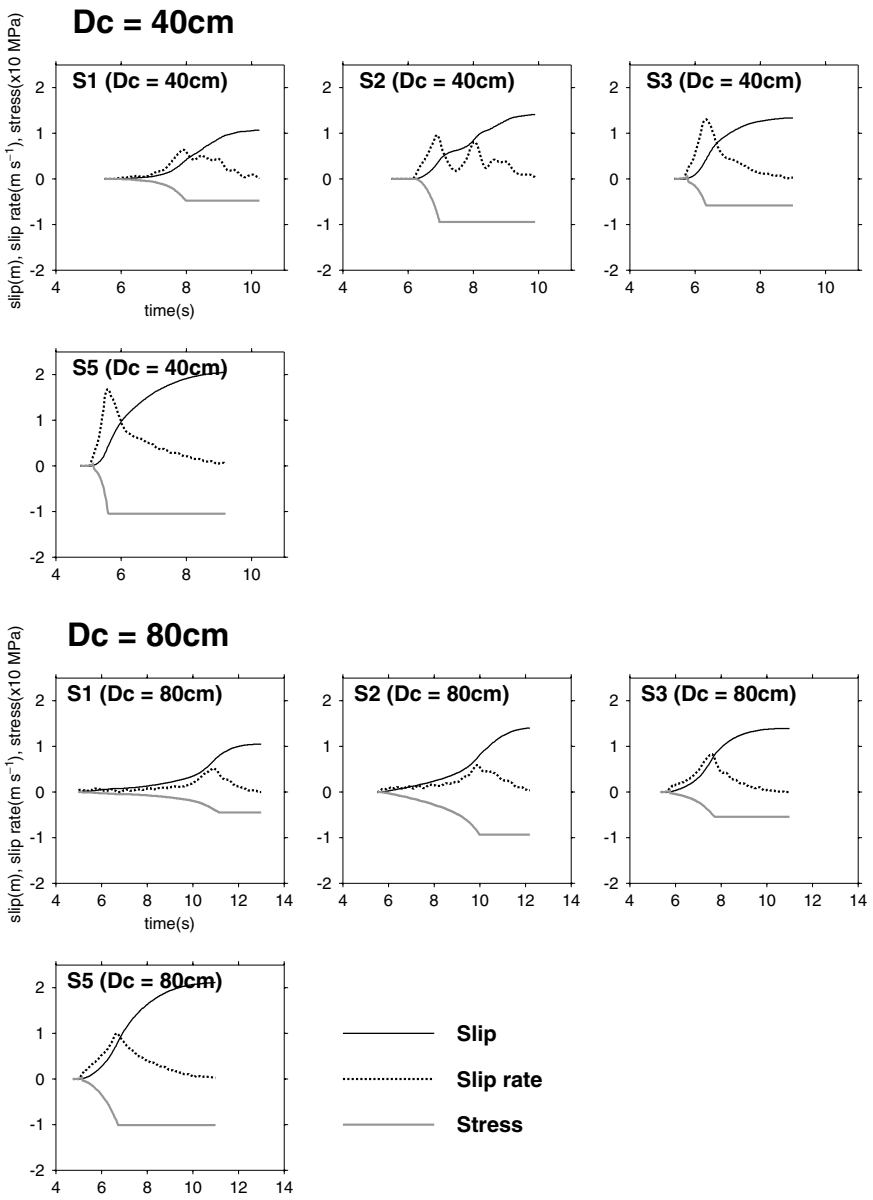

Figure 7. Time histories of stress change, slip and slip velocity at selected points, obtained from dynamic calculations for two prescribed values of $D_c = 40$ and 80 cm.

Additional theoretical constraint

There is another theoretical constraint in estimating the slip-weakening distance D_c. The breakdown zone length at the rupture front is related to the critical length L_c (see, for example, Ohnaka 2000), which may be approximated by D_c divided by half the strain drop as, $L_c \sim D_c/(\Delta\sigma/\mu)$ (S. Day, personal communication, 2002). Since the stress-breakdown time T_c is given by L_c/v, we obtain,

$$D_c = cT_c\Delta\sigma_b/\rho\beta, \tag{2}$$

where $\Delta\sigma_b$ is the breakdown stress drop, ρ is the density of the medium, v and β are the rupture velocity and shear wave velocity, respectively, and c is a numerical constant close to unity. The above relation can also be derived from eq. (50) in Ohnaka & Yamashita (1989). Eq. (2) means that the slip-weakening distance may also be roughly estimated from the stress drop if we measure T_c. Since $T_c = T_b - T_r$, and the time from the rupture arrival to the time of peak slip velocity $T_c' = T_{pv} - T_r$ (see Fig. 5b), then $T_c \sim T_c'$ if T_b can be approximated by T_{pv} as shown in the previous section. T_c' in the slip-velocity function obtained during the kinematic inversion ranges between 1.25 and 3.10 s. We tentatively replace the breakdown stress drop $\Delta\sigma_b$ by the dynamic stress drop $\Delta\sigma$, because the breakdown drop including the strength excess may not be well resolved. Combining the stress drop shown in Fig. 4 with T_c', we obtain the spatial distribution of D_c on the fault except for the numerical constant c, because ρ and β in the zone of the in-slab fault are already known. In Fig. 9 we plot the previously estimated D_c' values versus D_c calculated from eq. (2) using $\Delta\sigma$ and T_c. Although these points scatter over a rather wide range, we see that c is in the range between 0.4 and 0.8. These results suggest that the approach taken in the present study provided a better-resolved slip-weakening distance D_c than from the indirect estimate of using the stress drop and T_c, and that the theoretical constraint described here gives the upper bound of the real values of D_c. The upper bound of D_c in

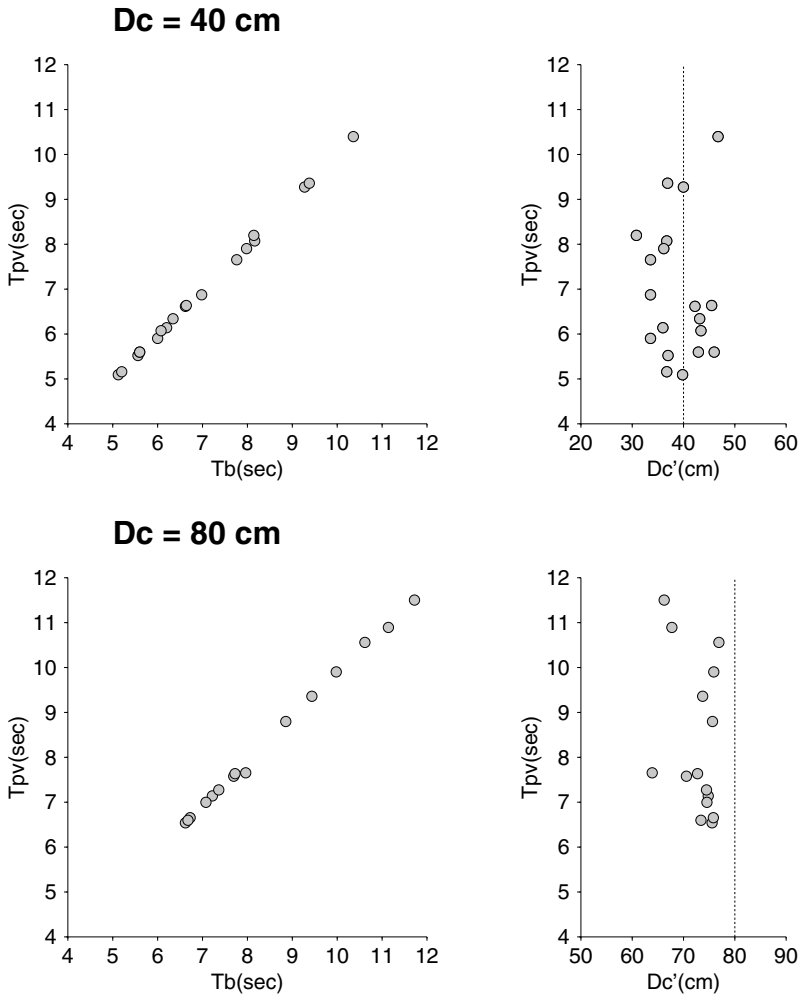

Figure 8. Relations between T_{pv} and T_b (left), and between T_{pv} and D_c' (right) for the case shown in Fig. 8, where T_b and T_{pv} are measured from the origin time at the rupture starting point.

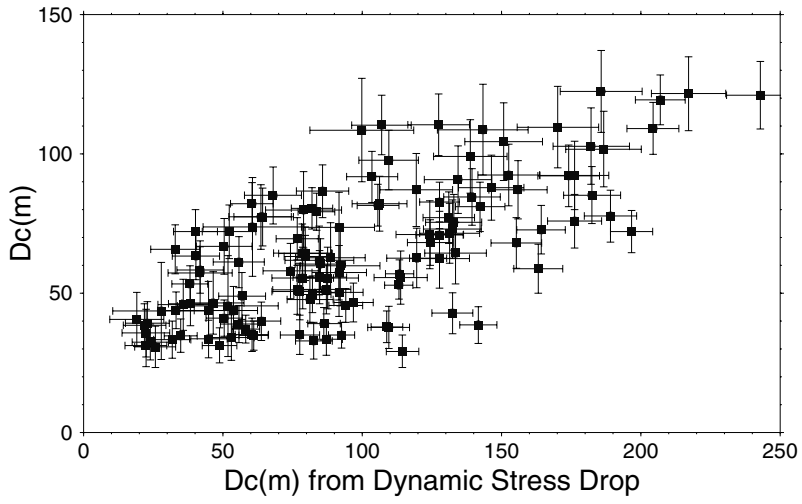

Figure 9. D_c values estimated from the slip-velocity functions plotted versus those calculated from a theoretical constraint $D_c = cT_c\,\Delta\sigma_b/\rho\beta$. In these plots, c is in the range between 0.4 and 0.8.

the large stress drop zone in the central fault section will be about 150–180 cm, if we assume $c \sim 0.8$.

Resolution and probable errors of the estimated D_c values

As a next step, we estimate the resolution and probable errors of the calculated D_c values, following the procedure taken by Mikumo *et al.* (2003). The resolution of D_c depends on the frequency bandwidth of the recorded waveforms (Fig. 2). The minimum resolvable value D_{cmin} would be $D_{cmin} = T_{cmin}\, V_{av} \sim T_{cmin} V_{max}/2$, if we refer to Guatteri & Spudich (2000), where T_{cmin} is the shortest modelled period involved in the waveform data, and V_{av} and V_{max} are the average slip velocity over T_{cmin} and the maximum slip velocity, respectively. For a filtering procedure for the observed waveforms, we applied a fourth-order Butterworth filter with a high-cut frequency of 0.5 Hz to the strong-motion records and of 1.0 Hz to the teleseismic records. The 0.5 Hz high-cut filter still retains amplitude levels of about 70 per cent at 0.5 Hz (or 2.0 s), 50 per cent at 0.67 Hz (or 1.5 s) and 25 per cent at 1.0 Hz (or 1.0 s). For this reason, we assume that the shortest period remaining on the filtered records, T_{cmin}, will be in the range between 1.0 and 1.5 s. V_{max} in the obtained slip-velocity function ranges between 30 and 105 cm s^{-1}. For these cases, D_{cmin} is estimated to be in the range between 15 and 53 cm, depending on the location on the fault. If we assume $T_{cmin} =$ 1.0 s, most of the estimated D_c values significantly exceed D_{cmin}. If we assume $T_{cmin} = 1.5$ s, instead, 18 out of 125 estimated D_c values would have to be discarded. However, many others are still above this higher, minimum resolvable limit.

On the other hand, the probable errors in estimating D_c come mainly from the precision of T_c' as expected from eq. (2),

$$\Delta D_c/D_c = \Delta T_c/T_c \sim \Delta T_c'/T_c'. \quad (3)$$

In the inversion procedure, we estimate a probable error of T_c' to be less than $0.25 + 0.05 = 0.30$ s, where the first value is a time-shift of the basis source time function and the second one is the sampling time interval of the slip-velocity functions. Since T_c' is in the range between 1.25 and 3.10 s, $\Delta D_c/D_c$ ranges from 10 to 40 per cent or $\Delta D_c = 11$–18 cm, depending on the location on the fault. Each point plotted in Fig. 9 has probable errors both in the vertical and horizontal axes.

We did not construct the stress-slip relations directly from the slip-velocity functions shown in Fig. 6, as has been tested in the previous study (Ide & Takeo 1997; Day *et al.* 1998; Mikumo *et al.* 2003). This is because some artefact would be introduced due to the finite grid size and the time increment used in this type of calculation, as has been shown by the resolution analysis made by Ide & Takeo (1997) for the 1995 Kobe earthquake.

Spatial distribution of D_c and G

The D_c values estimated here are plotted with their probable errors versus the local maximum slip in Fig. 10 to see whether there is any correlation between them. A few exceptional cases when $D_c - \Delta D_c < D_{cmin}$ are excluded from the figure. It can be seen that the median values of D_c ranging between 40 and 120 cm increase with the local maximum slip. If we exclude several estimates, almost all points appears to fall in the range $0.25 < D_c/D_{max} < 0.60$. However, if the product $T_{cmin} V_{av}$ is larger by a factor of 3 than assumed here, the minimum resolvable D_{cmin} would become larger and the above trend would be almost masked, although it seems unlikely.

In order to look at the spatial distribution of D_c, we tentatively divide the estimated values into four ranges, considering uncertainties in kinematic and dynamic calculations. Fig. 11 shows the spatial distribution of D_c in large-slip zones on the fault, which has been slightly smoothed by a Laplacian operator. For peripheral subfaults, the estimated values are less reliable due to small slip and slip velocities. Subfaults in the negative stress-drop zones are excluded because the slip-velocity functions have not been well resolved and also because our technique cannot be applied. From Fig. 11, we see that D_c in the central section with a maximum slip of 2.3 m exceeds 100 cm and sometimes reaches 120 cm, and that D_c in its right-downward section with a local maximum slip of 2.0–2.1 m also reaches 110–120 cm. Around these two zones, somewhat smaller D_c values of between 60 and 90 cm are distributed. In the zone around the hypocentre with a slip of 1.0–1.4 m and in the upper right-hand fault section, D_c is in the range of ~50–70 cm. Thus, the distribution does not indicate larger D_c values in shallow fault sections nor smaller D_c at deeper sections, but clearly shows a spatially heterogeneous distribution.

On the other hand, the breakdown stress drop $\Delta\sigma_b = \sigma_y - \sigma_f = \sigma_y - \sigma_0) + (\sigma_0 - \sigma_f)$ is roughly estimated on the large-slip zones. If we combine the estimated slip-weakening distance D_c with the breakdown stress drop $\Delta\sigma_b$, the fracture energy $G = \Delta\sigma_b\, D_c/2$, which is the effective surface energy to be the work done, may also

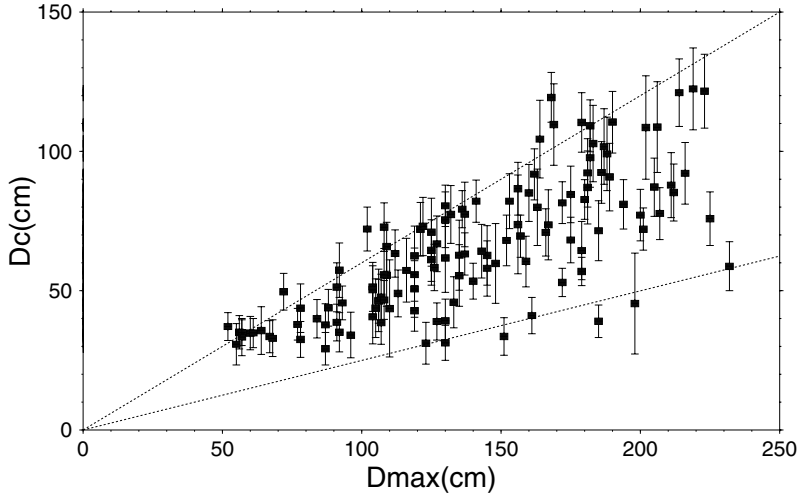

Figure 10. The estimated D_c values with their probable errors (thin vertical lines) plotted versus the local maximum slip on subfaults.

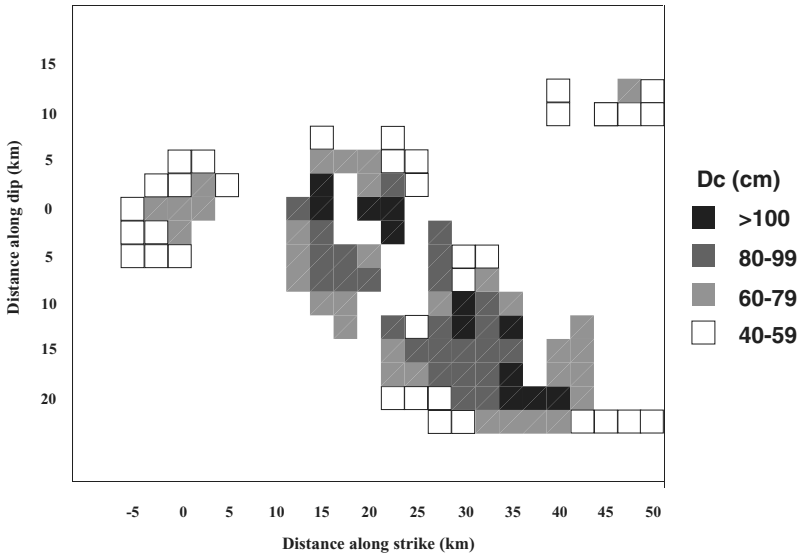

Figure 11. Spatial distribution of the estimated D_c values on the main part of the in-slab fault, which are classified into four ranges.

be roughly estimated. The estimated energy G in the central section and in the right-downward section ranges between 10 and 15 MJ m^{-2}, while it is about 5–8 MJ m^{-2} around the hypocentral zone.

1999 Tehuacan earthquake

The 1999 June 15 Tehuacan earthquake ($M_w = 7.0$) was located at 18.15°N and 97.52°W at a depth of 60 km from local and regional seismic observations (Singh *et al.* 1999). The source parameters determined from the moment tensor inversion of regional and teleseismic data by different institutions were: $\delta = 43°$–$46°$, $\phi = 290°$–$310°$, rake $= -82°$ to $-92°$ for the northward-dipping nodal plane, which is more likely to be the fault plane for a normal-faulting-type mechanism, in view of the duration of ground motion at near-field stations and the directivity of the recorded S waveforms (Singh *et al.* 1999). The estimated seismic moment ranges between 2.0 and 3.4 $\times$ 10^{26} dyn cm. A kinematic waveform inversion with simulated annealing algorithms has been made of 21 local strong-motion and regional broad-band records from seven stations (Iglesias 2001). The slip distribution obtained on the fault plane with dimensions of 60 $\times$ 60 km^2, which was divided into 64 subfaults, revealed two large-slip zones, one being located near the central fault section at depths between 60 and 75 km, and the other near the upper fault edge at depths of around 40 km. The maximum slip in the central zone was about 1.3 m. Another inversion analysis has also been performed with the 21 local and regional data and 15 teleseismic waveforms recorded at five stations (Quintanar *et al.* private communication, 2002). In this inversion, the basis source time function was expanded into five overlapping triangles, each having a half duration of 0.50 s with a time-shift of 0.50 s. The results show an almost similar slip distribution to the previous case, but without a large-slip zone near the upper fault edge.

Dynamic calculations incorporating the slip distribution yield a stress drop of about 110 bar in the central high-slip zones. From the above kinematic inversion, on the other hand, we estimate T_c' from the rupture arrival time to the time of peak slip velocity to be 1.3–1.5 s with a probable error of 0.5 s. If we apply eq. (2) to these values, tentatively assuming $c \sim 1.0$, the upper bound of the slip-weakening distance in the present case may be roughly estimated to be in the range between 95 and 110 cm in this high slip zone.

1997 Michoacan earthquake

The 1997 January 11 Michoacan earthquake ($M_w = 7.1$) was located at 18.09°N, 102.79°W at a depth of 35 km from local seismic observations. An inversion of teleseismic body waves (Santoyo *et al.* 2003), as well as two other moment tensor inversion, gave a nearly vertical faulting mechanism ($\delta = 87°$, $\phi = 105°$, slip $= -110°$), with a seismic moment of 4.5 $\times$ 10^{26} dyn cm. The kinematic waveform inversion (Santoyo *et al.* 2003) of four local strong-motion records together with 12 teleseismic data, provided the slip distribution on the vertical fault extending for a horizontal dimension of 45 km at a depth range between 20 and 50 km. In the inversion analysis, the entire fault was divided into 375 subfaults each with a dimension of 2 $\times$ 2 km^2, and a fixed rupture velocity of 2.80 km s^{-1} and a triangular source time function with a duration of 1.20 s were finally adopted, respectively, after many trial calculations. The results (Santoyo *et al.* 2003) show that a major slip larger than 2 m is concentrated at depths between 28 and 40 km, with a maximum slip exceeding 3 m. Dynamic rupture calculations (Mikumo *et al.* 2000) incorporating the above slip distribution revealed a stress drop higher than 200 bar, even up to 280 bar in a few localized zones, where a large slip was observed.

Since the kinematic inversion did not use a multitime window analysis, but assumed a single triangular source time function, it is difficult to estimate the time T_c' from the rupture arrival to the time of peak slip velocity at different locations on the fault, as in the case of the 1999 Oaxaca earthquake. However, it might be possible to assume the half duration of the source time function, $1.20/2 = 0.60$ s, as T_c'. This short time cannot be resolved by the present technique. Instead, if we apply eq. (2) to the present case, assuming $c \sim 1.0$, the upper bound of the slip-weakening distance D_c may be estimated to be in the range between 100 and 120 cm in the large stress drop zone.

3 DISCUSSION

In the present study, we estimated a probable range for the slip-weakening distance D_c on the in-slab fault of the 1999 Oaxaca, Mexico earthquake, following the approach proposed by Mikumo *et al.* (2003), which has been supported by the theoretical background (Fukuyama *et al.* 2003). Actually, our dynamic calculations for the in-slab fault with a heterogeneous stress drop distribution indicate that D_c at the stress breakdown time T_b can be well approximated in most cases by D_c' at the time of peak slip velocity $T_{pv,}$ as shown in Fig. 8. This relation is badly contaminated, however, at locations near the fault edges and strong barriers, as has been predicted by theoretical relations (Fukuyama *et al.* 2003). As has also been discussed in our previous paper, actual slip-weakening behaviour could be different from an idealized model proposed by Andrews (1976a,b), in which the shear stress is assumed to decrease linearly with ongoing slip up to the critical distance D_c. Numerical calculations of dynamic rupture propagation with different types of slip-weakening friction laws (Fukuyama *et al.* 2003) indicate that the deviations of D_c' from the prescribed value of D_c are within 20 per cent in most cases but sometimes reaches 50 per cent for the case of a very gentle decrease of shear stress. In addition, there are also observational uncertainties, including the limited frequency resolution of the recorded waveforms, which leads to the lowest resolvable value of D_c, and probable errors in measuring T_c' in the slip-velocity functions obtained from kinematic waveform inversion. Thus, it is to be mentioned that the slip-weakening distances estimated here should be regarded as those viewed from the frequency range limited between 0.05 and 0.5–1.0 Hz, and those located between the minimum resolvable limit and the upper bound of their real values.

Although our estimates have quite a large uncertainty as mentioned above, it is still interesting to note that the estimated D_c values appear to be spatially heterogeneous and dependent on the local maximum slip on the fault. These features are found to be similar to the case of shallow, vertical strike-slip earthquakes in Japan (Mikumo *et al.* 2003). This possible slip dependence of the critical slip-weakening distance might be interpreted by the roughness of fault surfaces (e.g. Okubo & Dieterich 1984; Ohnaka & Shen 1999), which appear to be distributed as a fractal-like structure (Scholz & Aviles 1986; Power *et al.* 1987), and/or the thickness of fault gouge layers (Marone & Kilgore 1993). Also to be noted here is that somewhat larger D_c values up to 120 cm are observed on the central section of the Oaxaca in-slab fault compared with those on the shallow fault of the two crustal events.

We also estimate the upper bound of the slip-weakening distance from a theoretical constraint between the breakdown stress drop $\Delta\sigma_b$ during the breakdown time T_c and D_c, as indicated in eq. (2). Comparing the D_c values estimated from the slip-velocity functions with those from the spatial distribution of $\Delta\sigma$ and T_c, a numerical constant c in eq. (2) appears to be in the range between 0.4 and 0.8, although this constant has a large uncertainty. If we tentatively assume $c \sim 1.0$ for the other in-slab, normal faulting earthquakes in the subducting Cocos plate, the upper bound of D_c values in the large stress drop zones would be about 110 cm for the 1999 Tehuacan earthquake and about 120 cm for the 1997 Michoacan earthquake, which are somewhat smaller than about 180 cm for the 1999 Oaxaca event. These estimated upper bounds are still larger than those calculated in the same way for the 2000 Tottori crustal earthquake. This difference might suggest the possible existence of a somewhat larger characteristic wavelength of the fault roughness on the in-slab fault surface due to higher normal stress in the subducting slab. On the other hand, laboratory experiments show that D_c also tends to increase with increasing temperature above 300 °C (Kato *et al.* 2003). This effect might also explain slightly larger D_c values for in-slab faults compared with crustal faults. The fracture energy estimated in the central fault section of the in-slab fault is also found to be larger by a factor of about 2 than that for the shallow crustal fault. For the same reason, the fracture energy needed to break asperities would be larger for the in-slab fault.

Although we should deal with many more earthquakes with different magnitudes, it seems that the above possible difference in the slip-weakening distance and the fracture energy between the in-slab and crustal faults may not be due to their scale effects with earthquake size but might be attributable to environmental effects.

4 CONCLUSIONS

We have estimated the critical slip-weakening distance during dynamic rupture on in-slab faults of normal-faulting earthquakes in the Mexican subduction zone, by applying a recent approach proposed by Mikumo *et al.* (2003), separately from the fracture energy or seismic radiation energy. For this purpose, we calculated the spatial distribution of slip-velocity functions and the final slip from a kinematic inversion of near-field strong-motion records and teleseismic waveforms in the frequency range between 0.05–0.5–1.0 Hz, and the stress time history and final stress change from dynamic calculations. The main conclusions we have obtained here are as follows.

(1) Dynamic calculations for a shear crack propagating on a dipping in-slab fault with a heterogeneous stress drop distribution show that the slip-weakening distance D_c at the stress-breakdown time T_b can be well approximated by the slip D_c' at the time of peak slip velocity T_{pv}, except at locations near strong barriers and fault edges.

(2) We found that the slip-weakening distance D_c reaches 120 cm in the central fault section and ranges between 50 and 70 cm around the hypocentre on the fault of the 1999 Oaxaca earthquake (M_w = 7.5), although these estimates have quite a large uncertainty.

(3) The estimated D_c values appear to be less depth-dependent but are rather more dependent on the local maximum slip. This possible slip dependence might be interpreted by the degree of fault roughness, in addition to stress heterogeneities.

(4) The fracture energy G in the central section and in the hypocentral zone are roughly estimated to be of the order of 10–15 and 5–8 MJ m^{-2}, respectively.

(5) Both of the estimated D_c and G values are somewhat larger than those on the vertical fault of two recent, shallow strike-slip earthquakes in western Japan. This difference might be due to the possible existence of a larger characteristic wavelength of the fault roughness and higher normal stress and higher temperature in the subducting slab than in the shallow crust.

ACKNOWLEDGMENTS

We are grateful to our colleagues, Kim B. Olsen and Eiichi Fukuyama who have made great scientific contributions, and Paul Spudich and Steve Day for their constructive suggestions to previous study on a similar topic. We wish to thank Steven N. Ward (Associate Editor), Ruth Harris and an anonymous reviewer for their comments that helped to improve the manuscript. The senior author also thanks Luis Quintanar and Arturo Iglesias for telling him about their results. The present work started with a joint research programme headed

by Masayuki Kikuchi between Mexican and Japanese groups. The broad-band and strong-motion data used in the present study are from the Servicio Sismologico Nacional, Instituto de Geofisica and Instituto de Ingenieria of the Universidad Nacional Autonoma de Mexico. This study is partly supported by the CONACyT (Mexico) project no 41209-F, for which we thank the assistance by Raul Valenzuela.

REFERENCES

Akaike, H., 1980. Likelihood and Beyes procedure, in *Beysian Statistics,* pp. 143–146, eds Bernardo, J.M., DeGroot, M.H., Lindley, D.V. & Smith, A.F.M., University Press, Valencia.

Andrews, D.J., 1976a. Rupture propagation with finite stress in antiplane, *J. geophys. Res.,* **81,** 3575–3582.

Andrews, D.J., 1976b. Rupture velocity of plane strain shear cracks, *J. geophys. Res.,* **81,** 5679–5687.

Campillo, M., Favreau, P., Ionescu, I.R. & Voisin, C., 2001. On the effective friction law of a heterogeneous fault, *J. geophys. Res.,* **106,** 16 307–16 322.

Clayton, R. & Engquist, B., 1977. Absorbing boundary conditions for acoustic and elastic equations, *Bull. seism. Soc. Am.,* **67,** 1529–1540.

Cocco, M., Pacheco, J.F., Singh, S.K. & Courboulex, F., 1997. The Zihuatanejo, Mexico, earthquake of 1994 December 10 ($M_w = 6.6$): Source characteristics and tectonic implications, *Geophys. J. Int.,* **131,** 135–145.

Day, S.M., 1982. Three-dimensional simulation of spontaneous rupture: the effect of nonuniform prestress, *Bull. seism. Soc. Am.,* **72,** 1881–1902.

Day, S.M., Yu, G. & Wald, D.J., 1998. Dynamic stress change during earthquake rupture, *Bull. seism. Soc. Am.,* **88,** 512–522.

Fukahata, Y., Yagi, Y. & Matsu'ura, M., 2003. Waveform inversion for seismic source processes using ABIC with two sorts of prior constraints: Comparison between proper and the improper formulations, *Geophys. Res. Lett.,* **30,** 10.1029/2002 GL016293

Fukuyama, E. & Madariaga, R., 1998. Rupture dynamics of a planar fault in a 3-D elastic medium: rate- and slip-weakening friction, *Bull. seism. Soc. Am.,* **88,** 1–17.

Fukuyama, E., Mikumo, T. & Olsen, K.B., 2003. Estimation of critical slip-weakening distance: Its theoretical background, *Bull. seism. Soc. Am.,* in press.

Guatteri, M. & Spudich, P., 2000. What can strong-motion data tell us about slip-weakening fault-friction laws?, *Bull. seism. Soc. Am.,* **90,** 98–116.

Hernandez, B. *et al.*, 2001. Rupture history of September 30, 1999 intraplate earthquake of Oaxaca, Mexico ($M_w = 7.5$) from Inversion of strong-motion data, *Geophys. Res. Lett.,* **28,** 363–366.

Ida, Y., 1972. Cohesive force across the tip of a longitudinal shear crack and Griffith's specific surface energy, *J. geophys. Res.,* **84,** 3796–3805.

Ide, S. & Takeo, M., 1997. Determination of constitutive relations of fault slip based on seismic wave analysis, *J. geophys. Res.,* **102,** 27 379–27 391.

Iglesias, A.M., 2001. Applicaciones del metodo de cristalizacion simulada a algunos problemas en sismologia, *MC tesis*, pp. 22–25, Instituto de Geofisica, UNAM.

Kato, N., Ohnaka, M. & Mochizuki, H., 2003, Constitutive properties for the shear failure of intact granite in seismogenic environments, *J. geophys. Res.,* in press.

Kikuchi, M. & Kanampori, H., 1991. Inversion of complex body waves—III, *Bull. seism. Soc. Am.,* **81,** 2335–2350.

Koketsu, K., 1985. The reflectivity method for synthetic near-field seismograms, *J. Phys. Earth,* **33,** 121–131.

Madariaga, R., Olsen, K.B. & Archuleta, R., 1998. Modeling dynamic rupture in a 3D earthquake fault model, *Bull. seism. Soc. Am.,* **88** 1182–1197.

Marone, C. & Kilgore, B., 1993. Scaling of the critical slip distance for seismic faulting with shear strain in fault zones, *Nature,* **362,** 618–621.

Matsu'ura, M., Kataoka, H. & Shibazaki, B., 1992. Slip-dependent friction law and nucleation processes in earthquake rupture, *Tectonophysics,* **211,** 135–148.

Mikumo, T. & Miyatake, T., 1993. Dynamic rupture processes on a dipping fault, and estimates of stress drop and strength excess from the results of waveform inversion, *Geophys. J. Int.,* **112,** 481–496.

Mikumo, T., Hirahara, K. & Miyatake, T., 1987. Dynamical fault rupture processes in heterogeneous media, *Tectonophysics,* **144,** 19–36.

Mikumo, T., Singh, S.K. & Santoyo, M.A., 1999. A possible stress interaction between large thrust and normal faulting earthquakes in the Mexican subduction zone, *Bull. seism. Soc. Am.,* **89,** 1418–1428.

Mikumo, T., Santoyo, M.A. & Singh, S.K., 2000. Dynamic rupture and stress change in a normal faulting earthquake in the subducting Cocos Plate, *Geophys. J. Int.,* **140,** 611–620.

Mikumo, T., Yagi, Y., Singh, S.K. & Santoyo, M.A., 2002. Coseismic and postseismic stress changes in a subducting plate: possible stress interaction between large interplate thrust and intraplate normal-faulting earthquakes, *J. geophys. Res.,* **107,** B1, ESE 5-1-5-12.

Mikumo, T., Olsen, K.B., Fukuyama, E. & Yagi, Y., 2003. Stress-breakdown time and slip-weakening distance inferred from slip-velocity functions on earthquake faults, *Bull. seism. Soc. Am.,* **93,** 264–282.

Miyatake, T., 1992. Reconstruction of dynamic rupture process of an earthquake with constraints of kinematic parameters, *Geophys. Res. Lett.,* **19,** 349–352.

Ohnaka, M., 2000. A physical scaling relation between the size of an earthquake and its nucleation zone size, *Pure appl. Geophys.,* **157,** 2259–2282.

Ohnaka, M. & Kuwahara, Y., 1990. Characteristic features of local breakdown near a crack-tip in the transition zone from nucleation to unstable rupture during stick-slip shear failure, *Tectonophysics,* **175,** 197–220.

Ohnaka, M. & Shen, L.-F., 1999. Scaling of the shear rupture process from nucleation to dynamic propagation: Implication of geometric irregularity of the rupturing surfaces, *J. geophys. Res.,* **104,** 817–844.

Ohnaka, M. & Yamashita, T., 1989. A cohesive zone model for dynamic shear faulting based on experimentally inferred constitutive relation and strong-motion source parameters, *J. geophys. Res.,* **94,** 4089–4104.

Ohnaka, M., Kuwahara, Y. & Yamamoto, K., 1987. Constitutive relations between dynamic physical parameters near a tip of the propagating slip zone during stick-slip shear failure, *Tectonophysics,* **144,** 109–125.

Okada, Y., 1992. Internal deformation due to shear and tensile faults in a half-space, *Bull. seism. Soc. Am.,* **82,** 1018–1040.

Okubo, P.G. & Dieterich, J.H., 1984. Effects of physical fault properties on frictional instabilities produced on simulated faults, *J. geophys. Res.,* **89,** 5817–5827.

Olsen, K.B., Madariaga, R. & Archuleta, R.J., 1997. Three-dimensional dynamic simulation of the 1992 Landers earthquake, *Science,* **278,** 834–838.

Olsen, K.B., Fukuyama, E. & Mikumo, T., 2003. Direct measurement of slip-weakening friction from near-fault strong motion data, *Bull. seism. Soc. Am.,* submitted.

Pardo, M. & Suarez, G., 1995. Shape of the subducted Rivera and Coccos plates in Southern Mexico, Seismic and tectonic implications, *J. geophys. Res.,* **100,** 12 357–12 373.

Papageorgiou, A.S. & Aki, K., 1983. A specific barrier model for the quantitative description of inhomogeneous faulting and the prediction of strong-ground motion, Part II. Applications of the model, *Bull. seism. Soc. Am.,* **73,** 953–978.

Peyrat, S., Olsen, K.B. & Madariaga, R., 2001. Dynamic modeling of the 1992 Landers earthquake, *J. geophys. Res.,* **106,** 26 467–26 482.

Power, W.L., Tullis, T.E., Brown, S.R., Boitnott, G.N. & Scholz, C.H., 1987. Roughness of natural fault surfaces, *Geophys. Res. Lett.,* **14,** 29–32.

Pulido, N. & Irikura, K., 2000. Estimation of dynamic rupture parameters from the radiated seismic energy and apparent stress, *Geophys. Res. Lett.,* **27,** 3945–3948.

Santoyo, M.A., Singh, S.K. & Mikumo, T., 2003. Source process of the 11 January, 1997 ($M_w = 7.1$) Michoacan, Mexico, normal faulting earthquake derived from local and teleseismic observations, *Bull. seism. Soc. Am.,* submitted.

Scholz, C. & Aviles, C.A., 1986. The fractal geometry of faults and faulting, in *Earthquake Source Mechanics,* Vol. 6, pp. 147–155, eds Das, S., Boatwright, J. & Scholz, C.H., Geophys. Monogr. 37, Maurice Ewing, Am. Geophys. Union.

Shibazaki, B. & Matsu'ura, M., 1998. Transition process from nucleation to high-speed rupture propagation: scaling from stick-slip experiments to natural earthquakes, *Geophys. J. Int.,* **132,** 14–30.

Singh, S.K., Astiz, L. & Havkov, J., 1981. Seismic gaps and recurrence period of large earthquakes along the Mexican subduction zone: a re-examination, *Bull. seism. Soc. Am.,* **71,** 827–843.

Singh, S.K., Suarez, G. & Dominguez, T., 1985. The Oaxaca, Mexico earthquake of 1931: lithospheric normal faulting in the subducted Cocos plate, *Nature,* **317,** 56–58.

Singh, S.K. *et al.*, 1999. A preliminary report on the Tehuacan, Mexico earthquake of June 15, 1999 ($M_w = 7.0$), *Seism. Res. Lett.,* **70,** 489–504.

Singh, S.K. *et al.*, 2000. The Oaxaca earthquake of 30 September 1999 ($M_w = 7.5$), A normal-faulting event in the subducted Cocos plate, *Seism. Res. Lett.,* **71,** 67–78.

Yagi, Y., Kikuchi, M. & Mikumo, T., 2001. Source rupture process of the September 30, 1999 Oaxaca, Mexico earthquake, and its relation the stress change due to a past earthquake, *Joint Meeting of Earth and Planetary Sciences of Japan, Tokyo*.